*MAT_291: A new micromechanics-inspired model for shape memory alloys

Jesper Karlsson[1], Stuart Kari[2], Rohit Dhume[2], and Shivram Kashyap[2]

[1]DYNAmore Nordic AB, Gothenburg, Sweden
[2]Medtronic plc, Minneapolis, MN 55432, USA

1 Introduction

This paper presents a new micromechanics-inspired constitutive model for shape memory alloys (SMAs) based on [1]. Shape memory alloys, e.g. Nitinol (Nickel-Titanium alloy), are widely utilized in the medical device industry because of their superelasticity. Superelastic properties of Nitinol enable its use in self-expanding stents and heart valve frames that can be inserted through a vein or artery using a thin delivery device and expanded at the target location. Motivated by the increased use of SMAs in the medical device industry, ***MAT_291** (***MAT_SHAPE_MEMORY_ALLOY**) is a first step towards more accurate and reliable material modeling. This material is currently available for solid elements and for explicit and implicit analysis.

SMAs consist of two solid crystallographic phases, austenite (a high symmetry crystal structure, stable at high temperatures) and martensite (a low symmetry crystal structure that can be twinned or de-twinned, stable at low temperatures). Reversible transformation between the different phases gives rise to the shape-memory effect and superelasticity. The former implies that seemingly permanent deformation in the martensite phase can be recovered upon transformation to austenite by heating. The latter implies the material can undergo large strains in tension which can be recovered upon unloading. However, the superelastic stress-strain cycle will show elastic hysteresis similar to rubber-like materials, resulting from the transformation between twinned martensite, detwinned martensite, and austenite, see Figure 1.
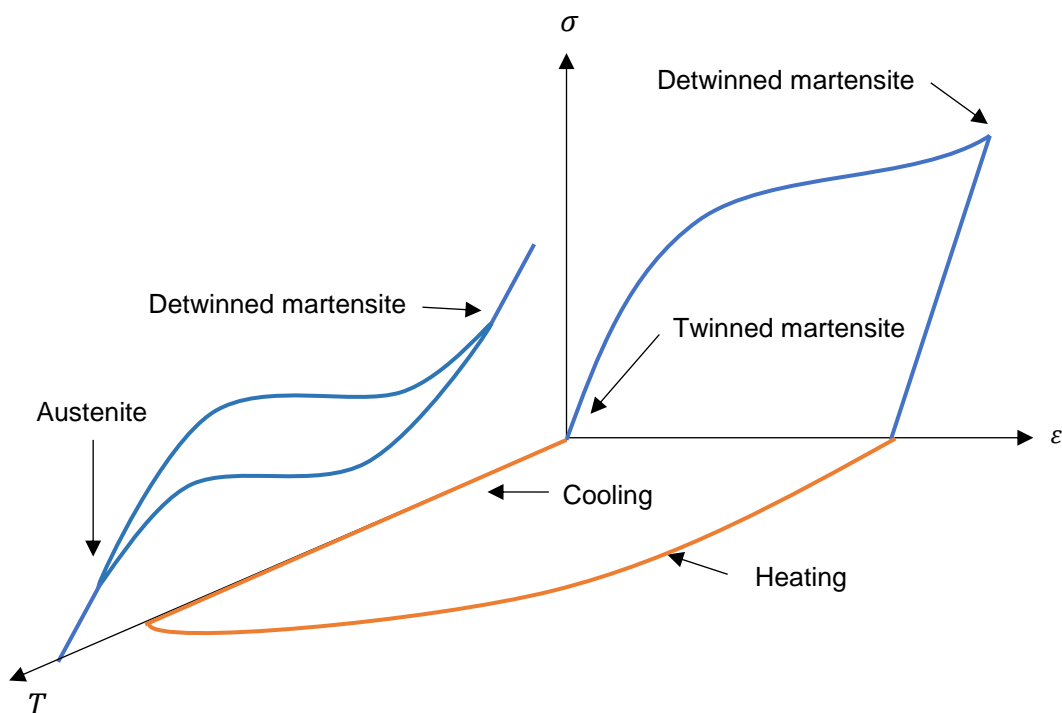

Figure 1: Phase transitions in SMAs.

Unlike phenomenological models, such as **MAT_30** (***MAT_SHAPE_MEMORY)** which is based on generalized plasticity [2], ***MAT_291** is based on a simple thermodynamic framework that boils down to

a single energy minimization problem, describing all possible phase transformations. In this model, the initiation and saturation of martensite are treated as two essentially different processes, governed by separate energy potentials that depend on two internal variables: the martensite volume fraction and the nominal martensite strain tensor. Also, fully coupled thermo-mechanical simulation has been enabled by extending ***MAT_THERMAL_ISOTROPIC_TD_LC** to incorporate the thermal energy contribution from ***MAT_291**.

2 Constitutive model

The model is based on minimizing the Helmoltz' free energy potential

$$W(\varepsilon, \varepsilon_m, \lambda, T) = \frac{1}{2}\varepsilon_e : \sigma + \lambda L \frac{T - T_c}{T_c} - c(\lambda)T\ln\left(\frac{T}{T_c}\right) + \lambda G_i(\varepsilon_m) + G_s(\lambda\varepsilon_m) + G_\lambda(\lambda),$$

where the total strain is assumed to be composed of elastic strain and martensite strain according to the additive split

$$\varepsilon = \varepsilon_e + \lambda\varepsilon_m,$$

and $0 \leq \lambda \leq 1$ is the volume fraction of martensite and ε_m is the (trace-free) nominal martensite strain describing the direction of grain growth. Note that this strain split allows a non-zero nominal martensite strain even if no martensite is present, i.e. $\lambda = 0$.

The first term in W is the strain energy density and the material is assumed to be isotropic elastic with

$$\sigma = C(\lambda) : \varepsilon_e,$$

where

$$C(\lambda) = \lambda C_m + (1 - \lambda)C_a,$$

is the effective stiffness that is a superposition of the martensite and austenite stiffness. The second term is the chemical energy density of martensite, linearized around the transition temperature T_c, and L is the latent heat of transformation. The third term is the thermal energy density where the heat capacity

$$c(\lambda) = \lambda c_m + (1 - \lambda)c_a,$$

is the linear combination of the heat capacities for martensite and austenite.

Finally, the last three terms describe energy densities for martensite initiation, saturation and transformation. In the simplest form, the potentials G_I and G_S are defined as

$$G_i(x) = k_i \cdot \max(g_i(x), 0)^{m_i+1}, \qquad i = I, S, \qquad k_i, m_i > 0,$$

where

$$g_i(x) = -1 + \frac{1}{b_i}\left[\left(\frac{1}{2}x : x\right)^{\frac{3}{2}} - a_i \det(x) - c_i \cdot |n^T x\, n|^3\right], \qquad i = I, S.$$

The set $\mathcal{G}_i = \{x : tr(x) = 0, g_i \leq 0\}$ indicates the set of admissible initiation or saturation strains where $b_i > 0$ is the radius, a_i is the tension-compression asymmetry, and c_i is the uniaxial asymmetry in the direction n. Inside $\mathcal{G}_i$, the volume fraction λ and martensite strain ε_m are allowed to vary freely without contribution to the energy. It is assumed that the parameters are chosen such that $\mathcal{G}_S \subset \mathcal{G}_I$. Lastly, the transformation energy and is defined as

$$G_\lambda(\lambda) = \frac{k_l \lambda^{m_l+1}}{m_l + 1}, \qquad k_l, m_l \geq 0.$$

Thus, the amount of stored energy in the system increase with increasing volume fraction.

Inside the sets of admissible strains, the evolution of λ and ε_m is governed by the additional kinetic relations

$$\dot{\lambda} = 0, \qquad if\ |d_\lambda| < d_\lambda^0,$$
$$d_\lambda\dot{\lambda} \geq 0,$$
$$|d_\lambda| \leq d_\lambda^0,$$

and

$$\dot{\varepsilon}_m = 0, \qquad\qquad if\ \|d_m\| < \lambda d_m^0,$$
$$d_m : \dot{\varepsilon}_m \geq 0,$$
$$\|d_m\| \leq \lambda d_m^0, \qquad if\ g_i(\varepsilon_m) \leq 0,$$

with driving forces

$$d_\lambda := -\frac{\partial W}{\partial \lambda}, \qquad d_m := -\frac{\partial W}{\partial \varepsilon_m}.$$

Here, the constants d_λ^0 and d_m^0 act as yield stresses, indicating the onset of martensite volume fraction and nominal martensite strain.

The stress σ and the entropy η are thermodynamic conjugates to ε and T through

$$\sigma = \frac{\partial W}{\partial \varepsilon}, \qquad \eta = -\frac{\partial W}{\partial T}.$$

Similarly, the driving forces d_λ and d_m are thermodynamic conjugates to λ and ε_m, and can be used to define the rate of dissipation

$$\dot{D} = d_\lambda \dot{\lambda} + d_{\varepsilon_m} : \dot{\varepsilon}_m \geq 0.$$

The above kinetic relations are then incorporated in the model by minimizing the mechanical energy

$$U = W + D,$$

over one time-step

$$\Delta U = \int_t^{t+\Delta t} \dot{U} ds = \int_t^{t+\Delta t} (\dot{W} + \dot{D}) ds = \Delta W + \int_t^{t+\Delta t} \dot{D} ds$$

$$\leq \Delta W + \int_t^{t+\Delta t} \left(d_\lambda^0 |\dot{\lambda}| + \lambda d_m^0 \cdot \|\dot{\varepsilon}_m\| \right) ds$$

$$\approx \Delta W + d_\lambda^0 |\lambda_{t+\Delta t} - \lambda_t| + \lambda_t d_m^0 \|\varepsilon_m^{t+\Delta t} - \varepsilon_m^t\|,$$

with respect to $\lambda_{t+\Delta t}$ and $\varepsilon_m^{t+\Delta t}$, see e.g. [1,3]. The evolution of λ and ε_m is thus constrained by the time step.

In conclusion, given previous values $\lambda^t, \varepsilon_m^t$ and the current strain $\varepsilon^{t+\Delta t}$, we find $\lambda^{t+\Delta t}, \varepsilon_m^{t+\Delta t}$ that minimize

$$W(\varepsilon, \varepsilon_m, \lambda, T) + d_\lambda^0 |\lambda_{t+\Delta t} - \lambda_t| + \lambda_t d_m^0 \|\varepsilon_m^{t+\Delta t} - \varepsilon_m^t\|.$$

The volume fraction λ and the nominal martensite strain ε_m are available as history variables.

3 Transition temperatures

At zero stress, the material will undergo phase transitions depending on four phase transition temperatures

$$M_f \leq M_s \leq A_s \leq A_f,$$

where M_f is the temperature where the austenite to martensite transformation is finished, M_s is the temperature where austenite begins to transform into martensite (cooling), A_s is temperature where martensite begins to transform into austenite (heating), and A_f is temperature where the martensite to austenite transformation is finished, see Figure 2.
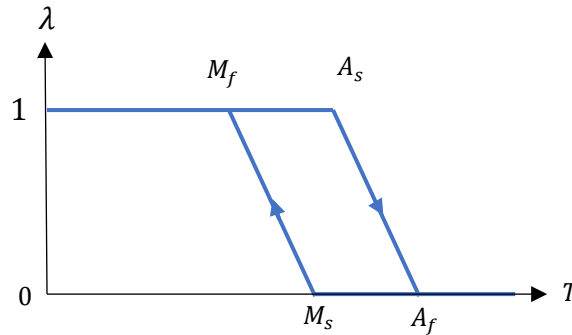

Figure 2: Transition temperatures in a heating-cooling cycle

These transition temperatures can be defined in ***MAT_291** and are related to the material parameters $d_\lambda^0, k_l, L,$ and T_c through the following expressions

$$M_s = T_c \left(1 - \frac{d_\lambda^0}{L} \right), \qquad M_f = T_c \left(1 - \frac{d_\lambda^0 + k_l}{L} \right),$$

$$A_s = T_c \left(1 + \frac{d_\lambda^0 - k_l}{L} \right), \qquad A_f = T_c \left(1 + \frac{d_\lambda^0}{L} \right).$$

4 Thermal balance

The internal energy is

$$\epsilon = W - \eta T,$$

and the internal energy rate is

$$\dot{\epsilon} = \dot{W} + \dot{T}\eta + T\dot{\eta} = \left(\sigma:\dot{\varepsilon} - d_m:\dot{\varepsilon}_m - d_\lambda\dot{\lambda} - \eta\dot{T}\right) + \dot{T}\eta + T\dot{\eta} = \sigma:\dot{\varepsilon} - d_m:\dot{\varepsilon}_m - d_\lambda\dot{\lambda} + T\dot{\eta}.$$

The energy balance can be written as

$$\dot{\epsilon} = \sigma:\dot{\varepsilon} - \nabla \cdot q + r,$$

where

$$q = -k\nabla T,$$

is temperature gradient and r is radiated heat.
Combining the above expressions gives

$$\nabla \cdot (k\nabla T) + r = \dot{\epsilon} - \sigma:\dot{\varepsilon} = -d_m:\dot{\varepsilon}_m - d_\lambda\dot{\lambda} + T\dot{\eta},$$

and using

$$\eta = -\frac{\partial W}{\partial T} = -\frac{\lambda L}{T_c} + c(\lambda)\left(1 + \ln\left(\frac{T}{T_c}\right)\right),$$

gives

$$\nabla \cdot (k\nabla T) + r = -d_m:\dot{\varepsilon}_m - d_\lambda\dot{\lambda} + T\left(-\frac{\dot{\lambda}L}{T_c} + c'(\lambda)\dot{\lambda}\left(1 + \ln\left(\frac{T}{T_c}\right)\right) + c(\lambda)\frac{\dot{T}}{T}\right).$$

Thus, the energy balance becomes

$$c(\lambda)\dot{T} = \nabla \cdot (k\nabla T) + r + Q,$$

with the volumetric heat generation

$$Q = \frac{TL}{T_c}\dot{\lambda} - Tc'(\lambda)\dot{\lambda}\left(1 + \ln\left(\frac{T}{T_c}\right)\right) + d_m:\dot{\varepsilon}_m + d_\lambda\dot{\lambda},$$

which is available as a history variable.

To facilitate coupled thermal analysis, **`*MAT_THERMAL_ISOTROPIC_TD_LC`** has been modified such that the heat capacity and thermal conductivity can be expressed with load curves HCLC/TCLC depending on λ, and the thermal generation can be input through a load curve TGRLC depending on Q.

5 Simple tensile test

Figure 3 shows the stress-strain curve for a single element tensile test at temperature $T > A_f$. The curve shows that the specimen is superelastic. Figure 4 shows the martensite volume fraction and martensite strain over time. Note that the martensite strain starts to develop before the onset of martensite.
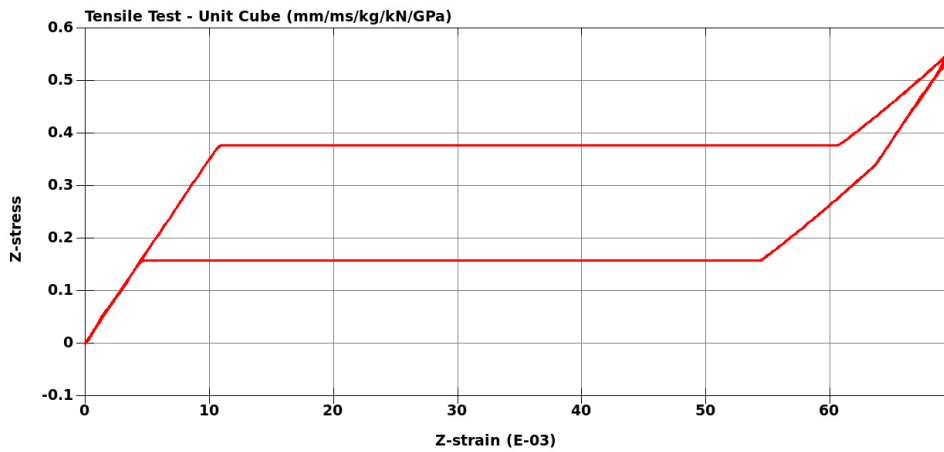

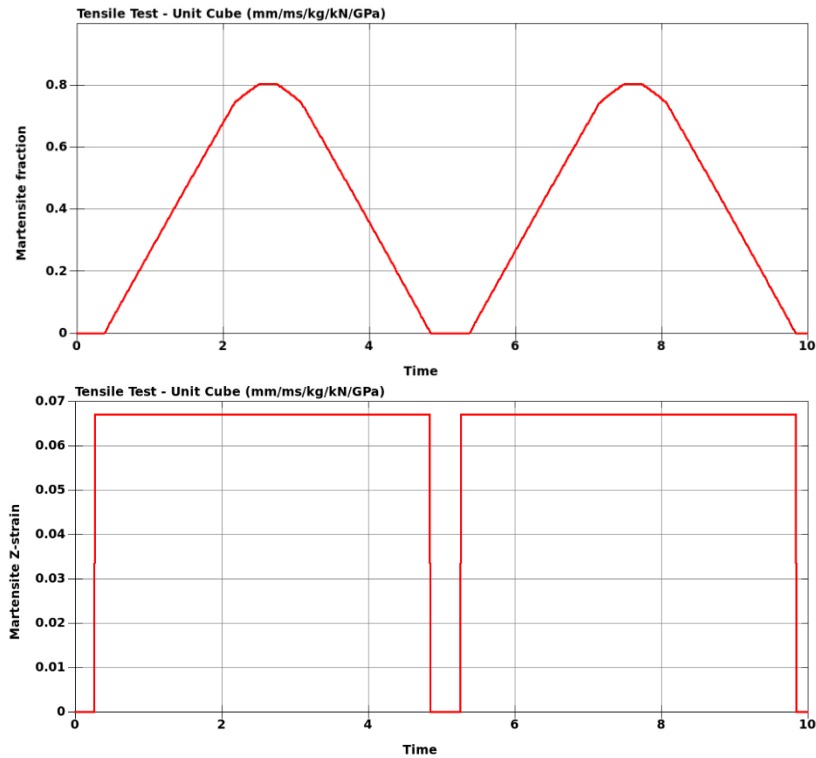*Figure 3: Stress-strain plot in the superelastic region for two strain cycles*

Figure 4: Martensite volume fraction λ and martensite strain ε_m

Figure 5 shows an actuation example for a temperature cycle during constant tensile loading. Here, $M_f = 100$K, $M_s = 150$K, $A_s = 250$K, and $A_f = 300$K. The thermal hysteresis from Figure 2 can be observed here.
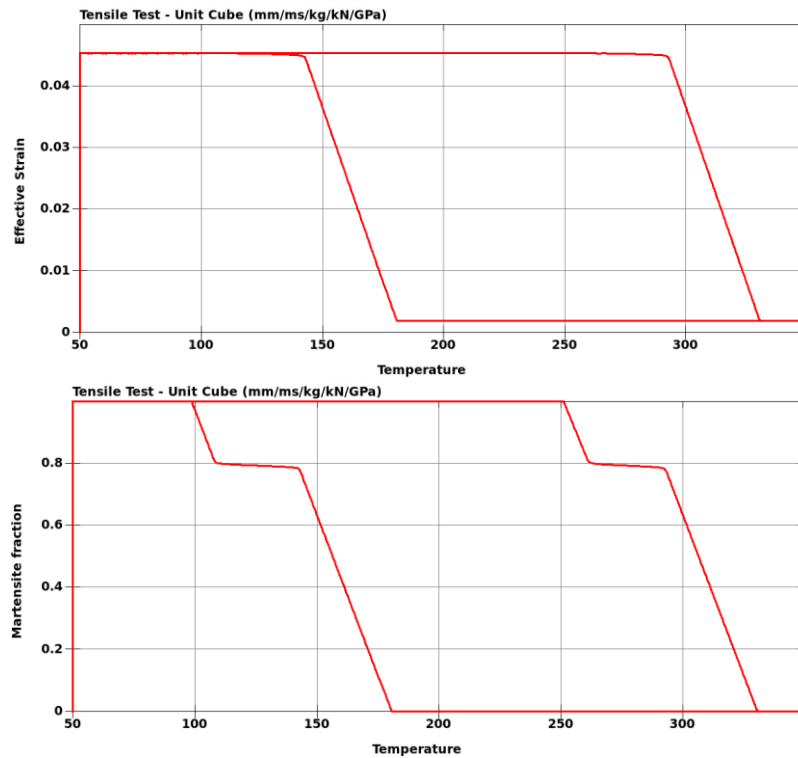

Figure 5: Actuation example showing thermal hysteresis

6 Paperclip example

We here show three different examples of deformation of a Nitinol paperclip modeled with solid elements. One end of the paperclip is fixed and the other is subjected to a displacement. In the first two examples, one low temperature and one high temperature example, the displacement is cyclic such that the end returns to its original coordinates. In the last example, the paperclip is first stretched, then the end is released, and finally the temperature is increased.

Figure 6 shows the first example where the paperclip undergoes a displacement cycle under low temperature $T < M_f$. The paperclip is in the martensite phase during the whole cycle and does not return to its original configuration. From Figure 7, showing the stress-strain cycle for a single element, it is apparent that there are residual strains and stresses at the end of the cycle.
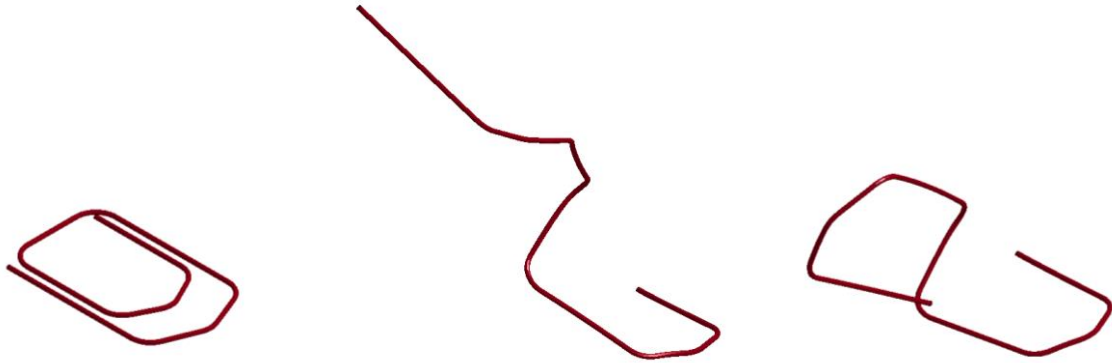
Figure 6: Deformation of paperclip at low temperature (beginning, middle and end of simulation)
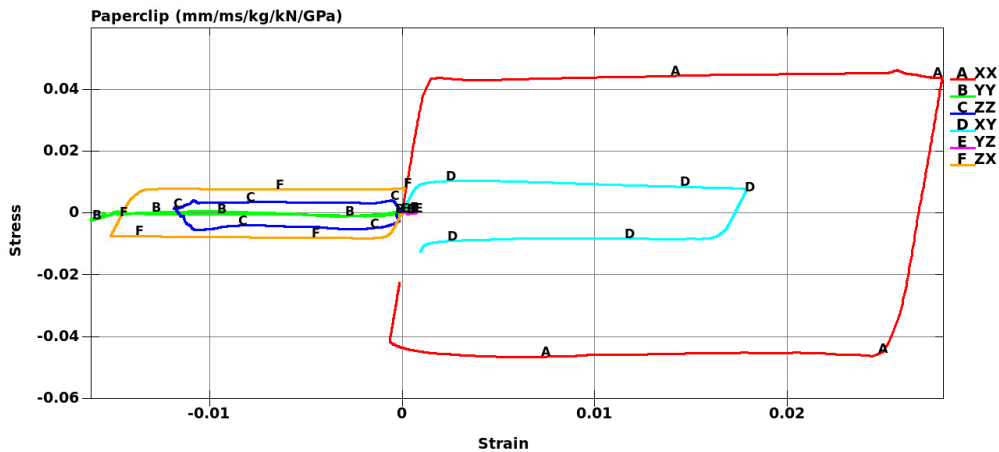

Figure 7: Stress-strain components for deformation of paperclip at low temperature

In the second example in Figure 8, the paperclip is subjected to the same displacements as in the first example, but at a high temperature $T > A_f$. The paperclip now returns to its original configuration without any residual strains and stresses, see Figure 9. Also, as shown in Figure 10, the paperclip now goes through a phase change, from austenite to martensite, under loading.
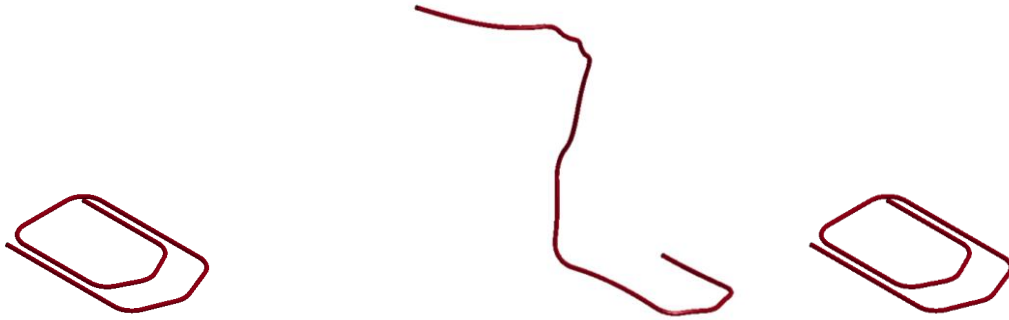
Figure 8: Deformation of paperclip at high temperature (beginning, middle and end of simulation)
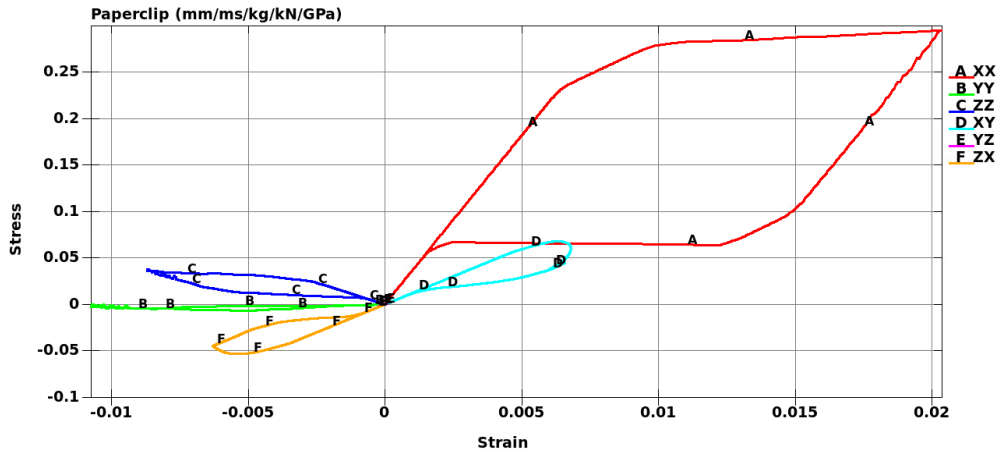

Figure 9: Stress-strain components for deformation of paperclip at high temperature
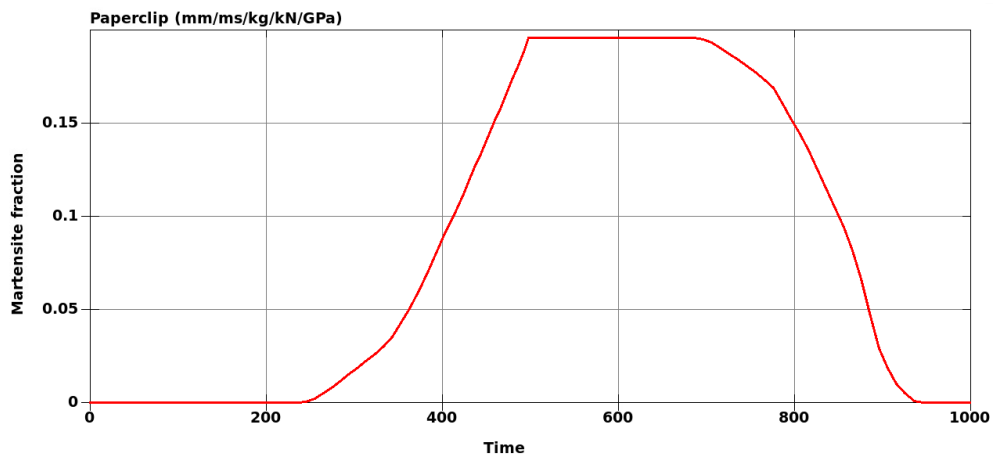

Figure 10: Martensite volume fraction for deformation of paperclip at high temperature

In the third example in Figure 11, the paperclip is first stretched until 500ms at low temperature $T < M_f$, then the end is released, and finally the temperature is gradually increased to $T > A_f$. The paperclip now returns to its original configuration without any residual strains and stresses, see Figure 13. Also, as shown in Figure 14, the paperclip now goes through a complete phase change, from martensite to austenite, under heating. Note that the return to the original configuration is a very fast process that happens during the sudden jump to austenite.
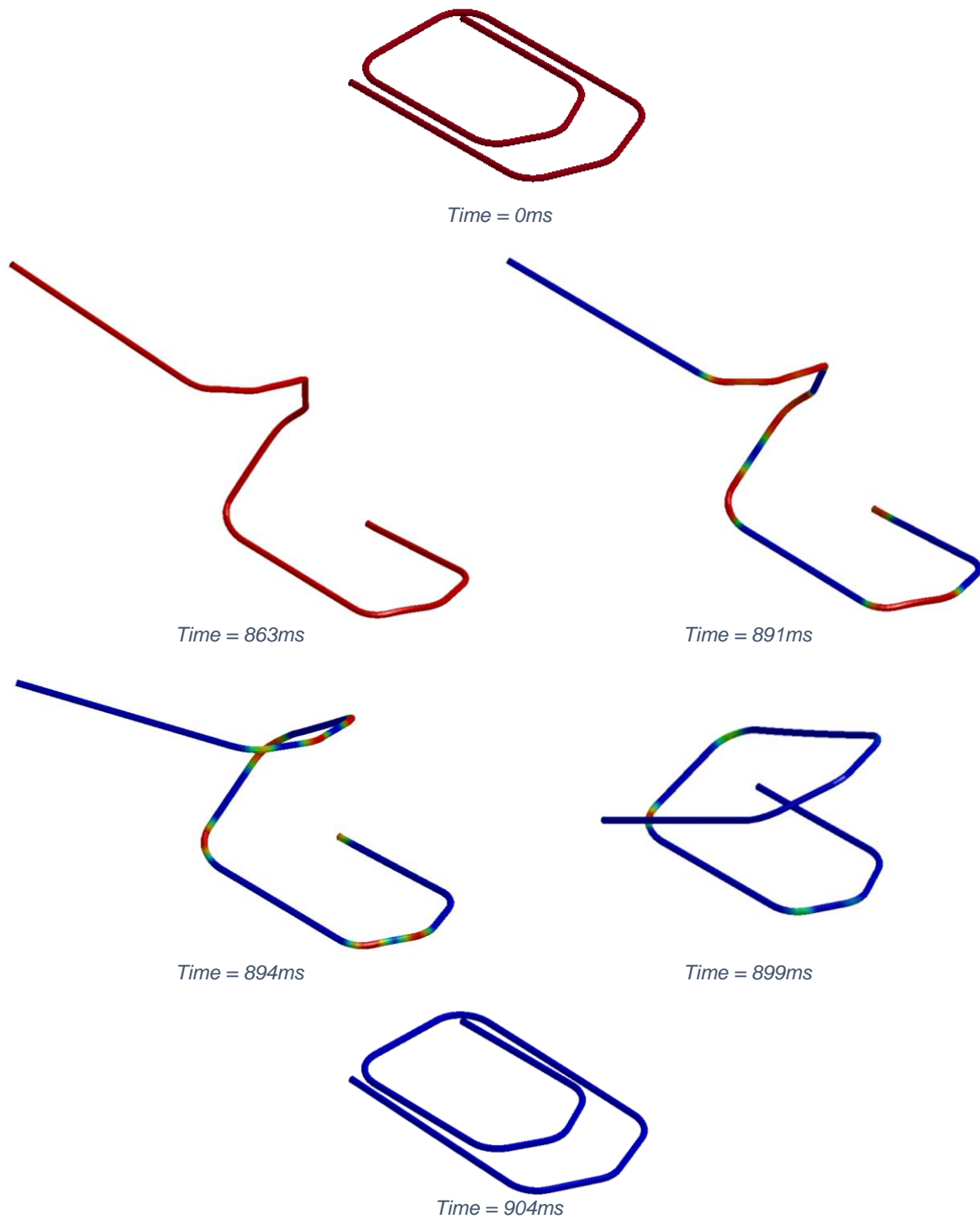
Figure 11: Deformation of paperclip under strain, relaxation and temperature change. Paperclip is stretched until time=500ms, then relaxed. Color indicates martensite volume fraction (red = martensite, blue = austenite). Only the initial configuration and the time steps at the phase change are shown. The paperclip returns to its original shape after heated to austenite phase.
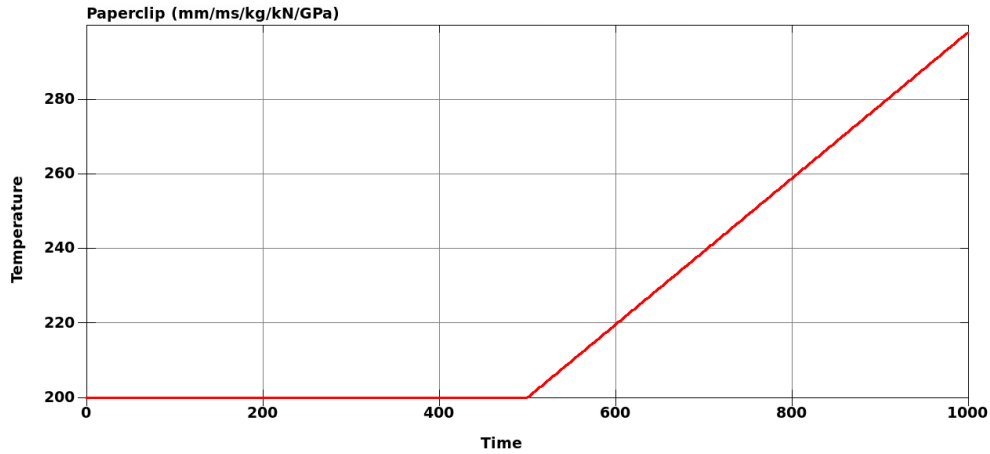
Figure 12: Temperature for deformation of paperclip under strain, relaxation and temperature change
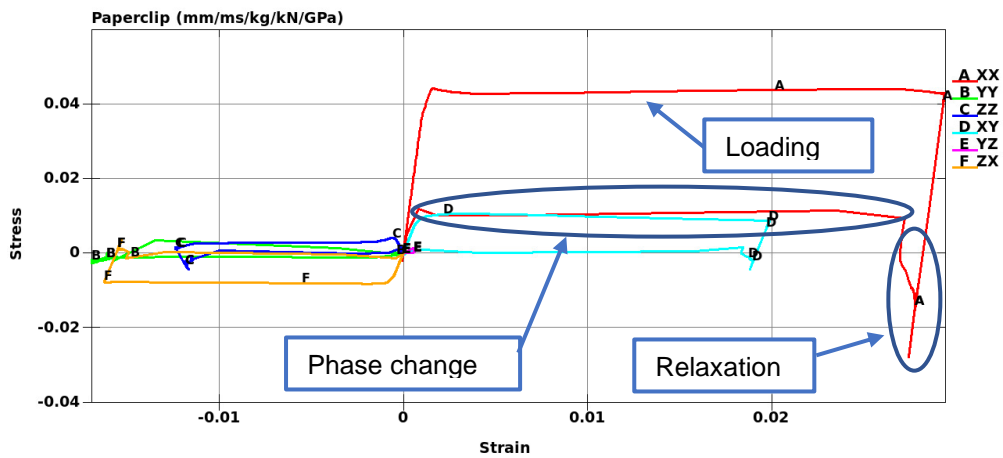

Figure 13: Stress-strain components for deformation of paperclip under strain, relaxation and temperature change
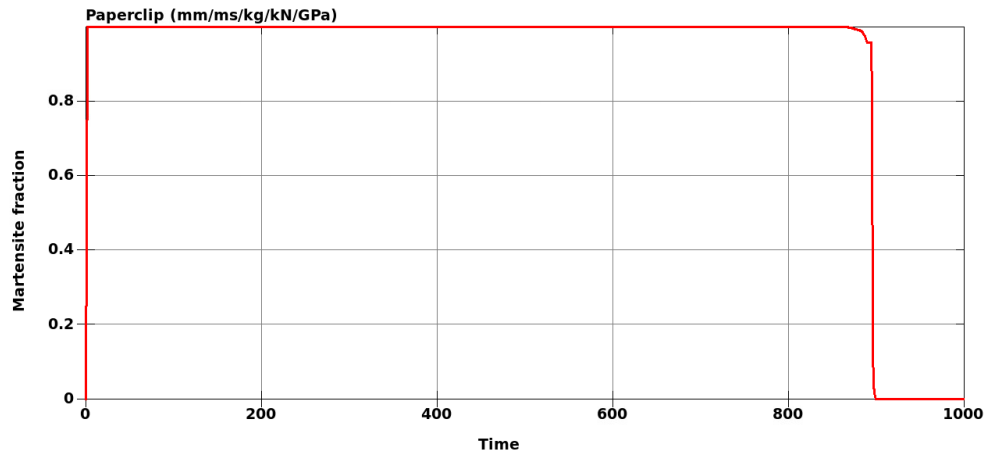

Figure 14: Martensite volume fraction for deformation of paperclip under strain, relaxation and temperature change

7 Conclusion

This paper presents the new material model ***MAT_SHAPE_MEMORY_ALLOY** for simulation of shape memory alloys. The constitutive model is based on energy minimization and the material is available for solid elements and for explicit and implicit analysis. Coupled thermal analysis is facilitated through a modification of ***MAT_THERMAL_ISOTROPIC_TD_LC** that makes use of the mechanical material history variables in ***MAT_SHAPE_MEMORY_ALLOY**.

8 References

[1] Kelly A., Stebner A. P., Bhattacharya K. "A micromechanics-inspired constitutive model for shape-memory alloys that accounts for initiation and saturation of phase transformation", Journal of the Mechanics and Physics of Solids 97 (2016) 197–224.

[2] Auricchio F., Taylor R. L., Lubliner J., "Shape-memory alloys: macromodelling and numerical simulations of the superelastic behavior", Comput. Methods Appl. Mech. Engrg. 146 (1997) 281-312.

[3] Junker, P., Makowski, J. & Hackl, K., "The principle of the minimum of the dissipation potential for non-isothermal processes", Continuum Mech. Thermodyn. (2014) 26: 259.